www.ietdl.org

Published in IET Microwaves, Antennas & Propagation
Received on 31st October 2011
Revised on 19th October 2012
Accepted on 13th November 2012
doi: 10.1049/iet-map.2012.0208

ISSN 1751-8725

Generalised method of current excitation reconstruction from near-field data of planar, cylindrical and spherical antenna arrays

Ritika Sen, Thomas D. Jerome-Surendran, Dhara Kiritkumar Trivedi, Mazher Abdul Qayyum, Balasubramaniam Preetham Kumar

Department of Electrical and Electronic Engineering, California State University, 6000 J Street, Sacramento, CA-95819-6019, USA
E-mail: kumarp@ecs.csus.edu

Abstract: Currently chemotherapy, radiation and surgery are the widely accepted treatments for cancer. A fourth modality, hyperthermia, or heat treatment, is emerging as an adjuvant cancer treatment along with radiation or chemotherapy, and works as a booster, sometimes even doubling the effects of these standard treatments. Hyperthermia essentially heats the cancer region to around 42°C by precisely controlled electromagnetic radiation in the 27, 900 or 2400 MHz frequency range. The re-emergence of hyperthermia is primarily due to advanced antenna technology, which can precisely target the tumour volume, while delivering minimal energy to neighbouring healthy tissue. The precise focusing of the electromagnetic beam is realised either by focusing plates or lenses, or by conformal antenna arrays. In order to achieve efficient array near-field control for hyperthermia applications, electronic control of the array currents is essential to control the beam over the tumour volume and achieve uniform heating. This paper reports a generalised analytical technique to reconstruct the array currents from a specific near-zone electric field profile. This reconstruction technique is applicable to conformal arrays with planar, cylindrical or spherical geometry. Several simulations have been carried out to test the validity and accuracy of the reconstruction algorithm.

1 Introduction

Near-field synthesis techniques find applications in diverse fields of medical therapy and communication systems. Applications in medical therapy are focused on heat treatment of tumours by focused hyperthermia, while in communication satellite systems, near-field techniques are used to detect defective elements in large array systems. These applications are elaborated in the section below.

1.1 Applications of near-field synthesis techniques

Antenna array synthesis techniques are very useful in the medical field, specifically related to the treatment of tumours by focused microwave or radiofrequency (RF) radiation. This method of focusing the beam by feeding the needed currents offers more controlled way of dealing with carcinoma using microwave hyperthermia [1–3]. A conformal array, with the precise current distribution can focus the antenna beam very precisely in the tumour-affected volume, with minimal radiation over the neighbouring healthy tissue [4–7]. Accurate beam steering of the radiation is also essential to obtain uniform heating over the tumour surface or tumour volume, depending on the tumour constituency.

Another application of near-field array synthesis pertains to the space communication field, where satellites usually work with large antenna array systems. In case any one antenna or few antennas malfunction, it becomes a tedious task to find the defective antennas among the large number of antennas. To solve this problem all the antennas on the satellite can be fed with currents and the currents reconstructed back from near-field data [8–11]. The non-defective antennas have the same reconstructed and initial currents. Those antennas for which the initial and reconstructed currents do not match are considered defective. Hence, this method is very effective to weed out the defective antennas when dealing with large number of antennas [8, 9]. However, the methods presented [8–11], for defective element detection, involve transformation of the measured near-field to the far-field, and then reconstruction of equivalent magnetic currents in the source plane [10] or iterative techniques based on Fast Fourier Transform (FFT) algorithms [11]. The essential difference in our reconstruction approach is a direct inversion of near-field of a conformal array source, with pre-specified geometry, as in a hyperthermia system. Since array current reconstruction will have to be done on a real-time basis for such a working therapy system, an algorithm with lesser complexity and computation stages would be advantageous.

1.2 Near-field focusing using conformal array technology

Coming back to the primary role in cancer treatment, tumours have traditionally been targeted by using radiation, chemotherapy and surgery, but alternative treatments for cancer are in the pipeline. Among the latter, Hyperthermia treatment is one of the more promising modalities against cancer, and in current times, it is transitioning from the experimental to clinical stage [1–3]. The mechanism behind hyperthermia therapy is based as follows: heating of cancer tissue by incident RF or microwave radiation sensitises the cells to the following radiation or chemotherapy treatment, sometimes even doubling the response, as compared with standalone radiation or chemotherapy [3]. Hence, hyperthermia treatment for cancer currently serves as a supplemental or adjuvant to chemotherapy or radiation, and this treatment is administered by using antenna arrays to focus RF or microwave energy to heat the area of the cancer tissue up to the desired temperature of 42°C (112°F).

For efficient hyperthermia application, it is necessary for the projected microwaves to be focused on the tumour area without having significant energy distributed over normal (non-cancerous) tissue and also to have control over the motion of the beam around the tumour area for successful therapeutic effect. In order to achieve this, the appropriate distribution of currents to the antenna array needs to be supplied; to generate accurately positioned radiation beams.

We need to remember that we are treating humans and animals; therefore the areas of the surface required to be treated can be of a various shapes. Therefore the array geometry being considered in this aspect has to be preferably conformal to planar, cylindrical and spherical surfaces [12–15]. Fig. 1 depicts typical surfaces of the body that can be applied with one of the three mentioned geometries.

An array that can generate any of the three shapes can be realised with a flexible microstrip patch material, as shown in Fig. 2*a* [14], or a set of waveguide elements housed in an outer frame [15], as shown in Fig. 2*b*, with fixed cross-sectional positions, but variable lateral position.

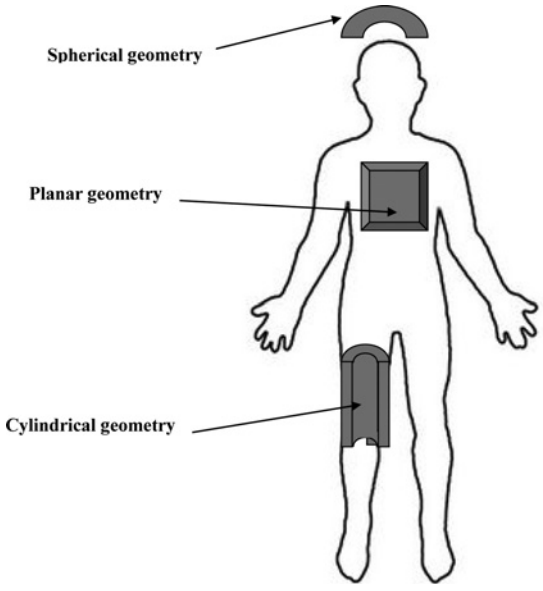

Fig. 1 *Array geometry application to typical hyperthermia sites*

Now by processing the reconstruction algorithm for each of these shapes individually, as described in this study, we can synthesise the array currents from the near-zone electric field information. Once calculated, these currents can be electronically controlled by the array, with the principal aim to focus on the desired tumour area. Sections 2–4 will outline the generalised element current reconstruction algorithm for planar, cylindrical and spherical array geometries.

1.3 Near-field focusing using continuous source technology

An alternate approach to obtaining a precise beam in the near field is to use focusing plates or lenses [16]. The latter paper describes one such technique to design near-field focusing plates, with the ability to produce a desired sub-wavelength focal pattern. A detailed four-step design procedure is presented in this paper, which concludes that completely passive near-field plates composed of inductive and capacitive elements can focus electromagnetic energy to extreme sub-wavelength dimensions.

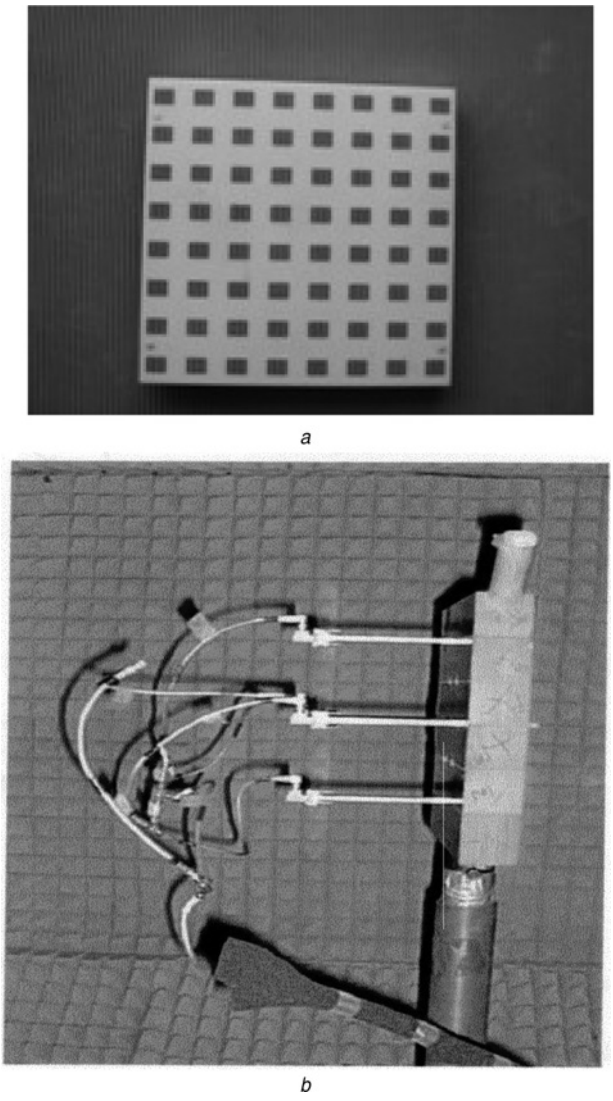

Fig. 2 *Conformal antenna array structures*

a Microstrip patch array [14]
b Waveguide array [15]

While focusing plates and lenses are also good options to obtaining near-field beams for possible hyperthermia applications, digital array control has greater flexibility in controlling the beam over the tumour area. In addition, array geometry can be controlled to conform to different body shapes and individual region profiles.

2 Synthesis of excitation currents of planar arrays

In the synthesis planar arrays, we utilise an inversion technique to reconstruct the excitation currents of planar arrays from near-field data, which is obtained over a planar surface close to the array. This technique is based on a two-dimensional FFT algorithm [17], and can be implemented with high accuracy and speed.

Let us consider a uniformly spaced planar array of M ***x***-directed electric point dipole elements, with an inter-element spacing d, and with as shown in Fig. 3.

Let there be $M = N^2$ number of elements in the array with N elements arranged along the x-axis (with y held constant) and N elements along the y-axis (for any fixed value of x). The exact expression for the near field of this array at an observation plane $P_1(x, y, z = z_0)$ obtained from the potential integral solution is given by Balanis *et al*.

$$E_x = -\mathrm{j}\omega A_x + \frac{1}{\mathrm{j}\omega\epsilon}\frac{\partial^2 A_X}{\partial x^2} \tag{1}$$

where A_x represents the magnetic vector potential. Simplifying the equation for A_x, we obtain

$$A_x = \frac{\mu}{4\pi}\sum_{m=0}^{M-1} a_m \frac{\mathrm{e}^{-\mathrm{j}ks_m}}{s_m} \tag{2}$$

where

$$s_m = \left[(x - x'_m)^2 + (y - y'_m)^2 + z^2\right]^{1/2} \tag{3}$$

and a_m is the amplitude and phase of the excitation current of the mth element located at $P(x'_m, y'_m, 0)$. Hence, simplifying (1), which is the dominant near-field component

$$E_x = \frac{-\mathrm{j}\omega\mu}{4\pi}\sum_{m=0}^{M-1} a_m \frac{\mathrm{e}^{-\mathrm{j}ks_m}}{s_m} + \frac{1}{4\pi\mathrm{j}\omega t}\sum_{m=0}^{M-1} a_m \mathrm{e}^{-\mathrm{j}ks_m} + \left[\frac{3\mathrm{j}k(x - x'_m)^2}{s_m^4} + \frac{3(x - x'_m)^2}{s_m^5} - \frac{\left[k^2(x - x'_m)^2 + 1\right]}{s_m^3}\frac{\mathrm{j}k}{s_m^2}\right] \tag{4}$$

The near field of the array reference element located to $x_0 = 0$; $y_0 = 0$ is given by [7]

$$E_{x_0} = \frac{-\mathrm{j}\omega\mu}{4\pi} a_0 \frac{\mathrm{e}^{-\mathrm{j}ks_0}}{s_0} + \frac{1}{4\pi\mathrm{j}\epsilon\omega} a_0 \mathrm{e}^{-\mathrm{j}ks_m}\left[\frac{3\mathrm{j}kx^2}{s_0^4} + \frac{3x^2}{s_0^5} - \frac{\left[k^2x^2 + 1\right]}{s_0^3} - \frac{\mathrm{j}k}{s_0^2}\right] \tag{5}$$

From (4) and (5) we obtain

$$E_X(x, y, z = z_0) = \sum_{m=0}^{M-1} a_m E_{X_0}(x - x_{m'}; y - y_{m'}; z_0) \tag{6}$$

By Fourier transforming (FT) on either side of (6) with respect to the spatial frequency variables 'u' and 'v', we obtain

$$\overline{E_x}(u, v) = \sum_{m=0}^{M-1} a_m \overline{E_{x_0}}(u, v)\mathrm{e}^{-\mathrm{j}kx'_m - \mathrm{j}vy'_m} \tag{7}$$

where

$$\overline{E_x}(u, v) = \iint_{-\infty}^{\infty} E_x(x, y)\mathrm{e}^{-jux - juy}\,\mathrm{d}x\,\mathrm{d}y \tag{8}$$

We rewrite (7) as

$$\overline{E_x}(u, v) = \overline{E_{x_0}}(u, v)\ \mathrm{FT}\left[a_m\right] \tag{9}$$

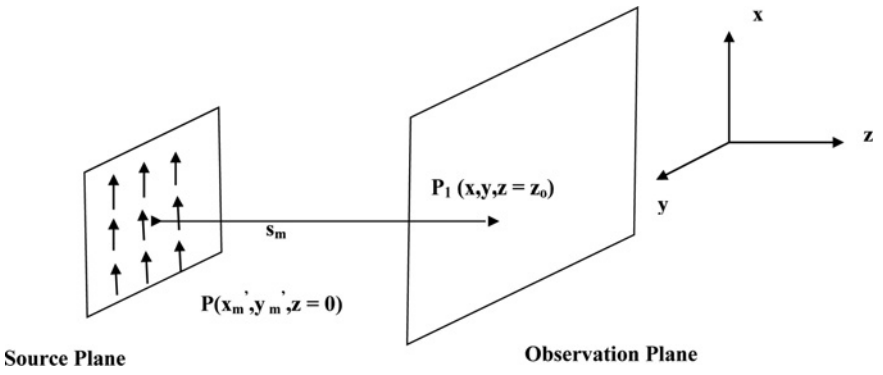

Fig. 3 *Rectangular array geometry and field plane*

doi: 10.1049/iet-map.2012.0208

and a_m denotes the x-directed surface current density of the radiating aperture. Following (9), we can obtain the current distribution, after taking the inverse FT.

3 Synthesis of excitation currents of cylindrical arrays

In this section, we present an efficient algorithm to synthesize the excitation currents of a circular cylindrical patch array, from near-field data over a concentric cylindrical surface [17]. Here, the geometry of the array is different, but the synthesis of array currents from near-field data is a similar two-dimensional Fourier inversion technique, as in the synthesis of planar arrays.

The circular cylindrical surface of a two-dimensional curved array is built up of discrete point dipole current elements distributed along the surface as depicted below in Figs. 4*a* and *b*. The spacing between the elements of the array is assumed to be uniform and the current flowing in the array elements is in the ϕ-direction as shown in Fig. 4*a* or in the z-direction as shown in Fig. 4*b*.

3.1 Discrete point dipoles with direction of current flow along ϕ-direction

The curved two-dimensional array has an inter-element spacing of dz in the z-direction and a spacing of dϕ along the ϕ-direction as depicted in Fig. 4*a*. The current element is considered to be located at a position $P_i(a, \phi_i, z_i)$, where a is the radius of the cylinder, whose surface current density is given by

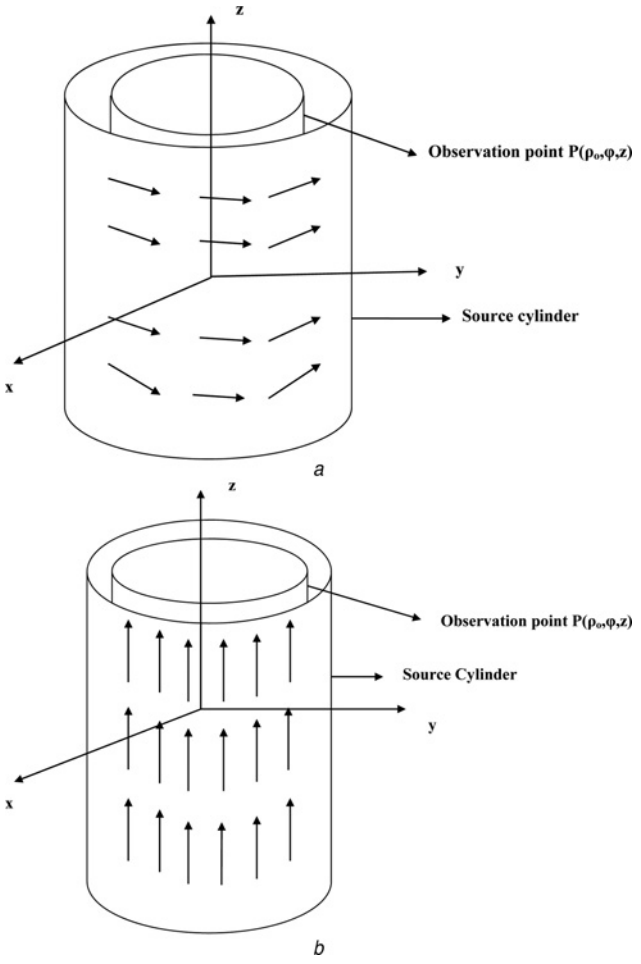

Fig. 4 *Geometry of cylindrical array*

a Array currents along ϕ-direction
b Array currents along $\hat{z}$-direction

$$\boldsymbol{J}_s = \hat{\boldsymbol{\phi}} \frac{\delta(z_i - z')\delta(\phi_i - \phi')I_i}{a} \tag{10}$$

where I_i is the excitation current of the ith array element. At the field observation position $P(\rho, \phi, z)$ in near field, we obtain the magnetic vector potential components as

$$A_{\rho i} = \frac{-I_i \sin(\phi_i - \phi)\mathrm{e}^{-\mathrm{j}k|\rho - \rho_i|}}{4\pi|\rho - \rho_i|} \tag{11a}$$

$$A_{\phi i} = \frac{-I_i \cos(\phi_i - \phi)\mathrm{e}^{-\mathrm{j}k|\rho - \rho_i|}}{4\pi|\rho - \rho_i|} \tag{11b}$$

where

$$|\rho - \rho_i| = \left[(x - x_i)^2 + (y - y_i)^2 + (z - z_i)^2\right]^{(1/2)} \tag{12}$$

or, in cylindrical coordinates

$$|\rho - \rho_i| = \left[\rho^2 + a^2 - 2\rho a \cos(\phi - \phi_i) + (z - z_i)^2\right]^{(1/2)} \tag{13}$$

The electric field at the near-field observation point, $P(\rho, \phi, z)$ is given by

$$E_i = \hat{\phi} E_{\phi i} + \hat{z} E_{zi} \tag{14}$$

Considering the individual ϕ-field component

$$E_{\phi i} = E_{1\phi i} + E_{2\phi i} \tag{15}$$

where

$$E_{1\phi i} = -\mathrm{j}\omega\mu A_{\phi i} \tag{16a}$$

and

$$E_{2\phi i} = \frac{1}{\mathrm{j}\omega\varepsilon\rho}\left[\frac{\partial}{\partial\rho}\ \frac{1}{\rho}\ \frac{\partial}{\partial\rho}(\rho_A \rho_i) + \frac{\partial^2 A_{\phi i}}{\partial\phi^2}\right] \tag{16b}$$

Considering the individual z-field component

$$E_{zi} = E_{1zi} + E_{2zi} \tag{17}$$

where

$$E_{1zi} = 0 \tag{18a}$$

and

$$E_{2zi} = \frac{1}{\mathrm{j}\omega\varepsilon\rho}\frac{\partial}{\partial z}\left[\frac{1}{\rho}\quad\frac{\partial}{\partial}\left(\rho_A\rho_i\right) + \frac{\partial^2 A_{\phi i}}{\partial z\partial\phi}\right] \tag{18b}$$

Defining the field expressions

$$L_i(\rho, \phi, z; a, \phi_i, z_i) = \frac{1}{\rho}\frac{\partial}{\partial\rho}\left(\rho_A\rho_i\right) \tag{19a}$$

$$M_i(\rho, \phi, z; a, \phi_i, z_i) = \frac{\partial}{\partial\rho}\left(\rho_A\rho_i\right) \tag{19b}$$

And defining the two-dimensional Fourier transform of the field components

$$\bar{A}_{\phi i}(\rho, u, v; a, \phi_i, z_i) = \int_0^{2\pi}\int_{-\infty}^{\infty} A_{\phi i}(\rho, \phi, z; a, \phi_i, z_i)\mathrm{e}^{-\mathrm{j}(u\phi+vz)}\,\mathrm{d}\phi\,\mathrm{d}z \tag{20a}$$

$$\bar{L}_i(\rho, u, v; a, \phi_i, z_i) = \int_0^{2\pi}\int_{-\infty}^{\infty} \mathrm{L}_i(\rho, \phi, z; a, \phi_i, z_i)\mathrm{e}^{-\mathrm{j}(u\phi+vz)}\,\mathrm{d}\phi\,\mathrm{d}z \tag{20b}$$

$$\bar{M}_i(\rho, u, v; a, \phi_i, z_i) = \int_0^{2\pi}\int_{-\infty}^{\infty} \mathrm{L}_i(\rho, \phi, z; a, \phi_i, z_i)\mathrm{e}^{-\mathrm{j}(u\phi+vz)}\,\mathrm{d}\phi\,\mathrm{d}z \tag{20c}$$

Using the Fourier transform relations, from 14 to 19, we obtain

$$\bar{E}_{zi} = \int_0^{2\pi}\int_{-\infty}^{\infty} E_{zi}(\rho, \phi, z)\mathrm{e}^{-\mathrm{j}(u\phi+vz)}\,\mathrm{d}\phi\,\mathrm{d}z = \frac{1}{\mathrm{j}\omega\varepsilon\rho}\left[\mathrm{j}v\bar{M}_0 - uv\bar{A}_{\phi 0}\right]I_i\mathrm{e}^{-\mathrm{j}u\phi_i-\mathrm{j}vz_i} \tag{21a}$$

and

$$\bar{E}_{\phi i} = I_i\left[-\mathrm{j}\omega\mu\bar{A}_{\phi 0} + \frac{1}{\mathrm{j}\omega\varepsilon\rho}\mathrm{j}u\bar{L}_0 - \frac{u^2}{\rho}\bar{A}_{\phi 0}\right]\mathrm{e}^{-\mathrm{j}u\phi_i-\mathrm{j}vz_i} \tag{21b}$$

where

$$\bar{M}_0 = \frac{\bar{M}_i(\rho, u, v; a, 0, 0)}{I_i} \tag{22a}$$

$$\bar{A}_{\phi 0} = \frac{\bar{A}_{\phi i}(\rho, u, v; a, 0, 0)}{I_i} \tag{22b}$$

given that $I_i \neq 0$

Finally, we have

$$\bar{E}_\phi(\rho, u, v) = \sum_{i=1}^{M}\bar{E}_{\phi i} = \left[-\mathrm{j}\omega\mu\bar{A}_{\phi 0} + \frac{1}{\mathrm{j}\omega\varepsilon\rho}\left\{\mathrm{j}u\bar{L}_0 - \frac{u^2}{\rho}\bar{A}_{\phi 0}\right\}\right]\sum_i I_i\mathrm{e}^{-\mathrm{j}u\phi_i-\mathrm{j}vz_i} \tag{23a}$$

$$\bar{E}_z(\rho, u, v) = \frac{1}{\mathrm{j}\omega\varepsilon\rho}\left[\mathrm{j}v\bar{M}_0 - uv\bar{A}_{\phi 0}\right]\sum_i I_i\mathrm{e}^{-\mathrm{j}u\phi_i-\mathrm{j}vz_i} \tag{23b}$$

Rewriting (23a) and (23b), we obtain the Fourier coefficients of the current distribution as follows

$$\sum_i I_i\mathrm{e}^{-\mathrm{j}u\phi_i-\mathrm{j}vz_i} = \frac{\bar{E}_\phi(\rho, u, v)}{\left[-\mathrm{j}\omega\mu\bar{A}_{\phi 0} + \left(1/(\mathrm{j}\omega\varepsilon\rho)\right)\left\{\mathrm{j}u\bar{L}_0 - \left((u^2)/\rho\right)\bar{A}_{\phi 0}\right\}\right]} \tag{24a}$$

and

$$\sum_i I_i\mathrm{e}^{-\mathrm{j}u\phi_i-\mathrm{j}vz_i} = \frac{\bar{E}_z(\rho, u, v)}{\left(1/(\mathrm{j}\omega\varepsilon\rho)\right)\left[\mathrm{j}v\bar{M}_0 - uv\bar{A}_{\phi 0}\right]} \tag{24b}$$

which can be inverse Fourier transformed to obtain the array currents $I_i(\varphi, z)$.

3.2 Discrete point dipoles with direction of current flow along $\hat{z}$-direction

Analysing current flow using a similar analysis employed previously in Section 3.1 gives us the following

$$\boldsymbol{J}_s = \hat{z}_i\frac{\delta(z - z_i)\delta(\phi - \phi_i)I_i}{a} \tag{25}$$

$$A_{zi} = \frac{I_i\mathrm{e}^{-\mathrm{j}k|\rho-\rho_i|}}{4\pi|\rho - \rho_i|} \tag{26}$$

and, adopting a similar analysis as in Section 3.1, we obtain the two-dimensional Fourier transform of the element near-zone electric field distribution as follows

$$\bar{E}_i(\rho, u, v; a, \phi_i, z_i) = \left[\hat{\phi}\left(\frac{1}{\mathrm{j}\omega\varepsilon}\right)\left(\frac{-uv}{\rho}\right)\bar{A}_{z0} + \hat{z}\left(-\mathrm{j}\omega\mu - \frac{v^2}{\mathrm{j}\omega}\right)\bar{A}_{z0}\right]I_i\mathrm{e}^{-\mathrm{j}u\phi_i-\mathrm{j}vz_i} \tag{27}$$

And, the two-dimensional Fourier transform of the array near-zone electric field distribution is finally obtained as

$$\bar{E}(\rho, u, v) = \sum_{i=1}^{M}\bar{E}_i(\rho, u, v; a, \phi_i, z_i) = \bar{A}_{z0}\left[\hat{\phi}\left(\frac{1}{\mathrm{j}\omega}\right)\left(\frac{-uv}{\rho}\right) + \hat{z}\left(-\mathrm{j}\omega\mu - \frac{v^2}{\mathrm{j}\omega\varepsilon}\right)\right]\sum_i I_i\mathrm{e}^{-\mathrm{j}u\phi_i-\mathrm{j}vz_i} \tag{28}$$

which can be inverted, as shown in Section 3.1 to yield the array current distribution, $I_i(\varphi, z)$.

doi: 10.1049/iet-map.2012.0208

4 Synthesis of excitation currents of spherical arrays

This section details the reconstruction algorithm to obtain the array currents from the near-field data of a spherical array. The analysis of spherical arrays is more complex than planar or cylindrical arrays, owing to the geometry. Hence, it does not involve a purely two-dimensional Fourier transform inversion as in the case of the planar and cylindrical arrays, but a Legendre–Fourier type of transformation [19, 20]. The following sections detail the analysis of the spherical array, and the inversion procedure to reconstruct the array currents for the near-field data.

4.1 Near-field analysis of spherical array

Consider a spherical array of N-point dipoles, as shown in Fig. 5, with array radius r_0. The array currents are directed outwards in the radial, r-direction.

The near-zone electric field of the array at an observation point $P(R, \theta, \varphi)$ is given by

$$E_r(\theta, \Phi) = \sum_{n=1}^{N} I(\theta_n, \Phi_n) f(\theta, \Phi, \Phi_n, \theta_n) \tag{29}$$

where

$$f(\theta, \Phi, \Phi_n, \theta_n) = \frac{1}{r}\frac{\partial}{\partial \Phi}\left[\frac{6}{4\pi}\frac{e^{-jkR}}{R}\right]$$

$$R = \sqrt{r^2 + r_0^2 + 2rr_0 \sin\theta \sin\theta_n + \cos\theta \cos\theta_n \cos(\Phi - \Phi_n)}$$

and

$$\frac{\partial}{\partial \Phi}\left[\frac{e^{-jkR}}{R}\right] = \frac{R(-jk)e^{-jkR}((\partial R)/(\partial \Phi)) - e^{-jkR}((\partial R)/(\partial \Phi))}{R^2}$$

$$\frac{\partial R}{\partial \Phi} = \frac{1}{2R}\left[\cos\theta \cos\theta_n \sin(\Phi - \Phi_n)\right]$$

Solving

$$f(\theta, \Phi, \Phi_n, \theta_n) = \frac{1}{8\pi R^3}[jkR + 1]e^{-jkR} \left[\cos\theta \cos\theta_n \sin(\Phi - \Phi_n)\right] \tag{30}$$

and the final equation for the electric field is

$$E_r(\theta, \Phi) = \sum_{n=1}^{N} I(\theta_n, \Phi_n)[jkR + 1]\frac{e^{-jkR}}{R^3} \left[\cos\theta \cos\theta_n \sin(\Phi - \Phi_n)\right. \tag{31}$$

where

$$R = \sqrt{r^2 + r_0^2 + 2rr_0 \sin\theta \sin\theta_n + \cos\theta \cos\theta_n \cos(\Phi - \Phi_n)}$$

4.2 Synthesis of excitation currents of the spherical array

From (29)

$$E_r(\theta, \Phi) = \frac{1}{4\pi r}\sum_{n=1}^{N} I_n \frac{\partial}{\partial \Phi}\left[\frac{e^{-jKR}}{R}\right]$$

Expanding the finite $[(e^{-jKR})/(R)]$ using spherical wave expansion [21] we obtain, for $r < r_0$ (see (32))
where $P_m^l(\cos x)$ is the associated Legendre function and $(J_{l+(1/2)})$, $(H_{l+(1/2)})$ are spherical Bessel functions. The synthesis procedure is shown below in a series of steps:
Step 1: Legendre Fourier Transform (see (33))
which finally yields

$$Q(n, m) = \frac{F(n, m) \cdot 8r^2 r_0 \cdot n(n+1) \cdot (n-m)! \cdot 4\pi}{H_{n+(1/2)}(kr0)J_{n+(1/2)}(kr)m(n+m)!} = \sum_{p=1}^{N} I_p P_n^m(\cos\theta_p)e^{-jm\varnothing p} \tag{34}$$

$P_l^{-m}(x)$ and $P_l^m(x)$ are proportional, and related by the following relation [19]

$$P_l^{-m}(x) = \frac{(-1)^m(l-m)!}{(l+m)!} P_l^m(x) \tag{35}$$

Step 2: Spherical harmonic representation

$$E_r(\theta, \Phi) = \frac{1}{4\pi r}\sum_{n=1}^{N} I_n \frac{\partial}{\partial \Phi}\left[\frac{\pi}{2jr\, r_0}\sum_{l=-\infty}^{\infty}\frac{2l+1}{l(l+1)}H_{l+(1/2)}(kr0)\, J_{l+(1/2)}(kr)\sum_{m=-l}^{l}\frac{(l-m)!}{(l+m)!}P_m^l(\cos\theta)P_m^l(\cos\theta_n)e^{jm(\varnothing-\varnothing_n)}\right]$$

$$= \frac{1}{8r_0 r^2}\sum_{n=1}^{N} I_n \sum_{l=-\infty}^{\infty}\frac{2l+1}{l(l+1)}H_{l+(1/2)}(kr0)\, J_{l+(1/2)}(kr)\sum_{m=-l}^{l} mP_m^l(\cos\theta)P_m^l(\cos\theta_n)e^{jm(\varnothing-\varnothing_n)} \tag{32}$$

$$F(n, m) = \int_0^{2\pi}\int_0^{\pi} E(\theta, \varnothing)\, P_l^m(\cos\theta)e^{-jm\varnothing}\sin\theta\, d\theta\, d\Phi = \frac{1}{8r^2 r_0}\sum_{p=1}^{N} I_p \frac{1}{n(n+1)}H_{n+(1/2)}(kr0)J_{n+(1/2)}(kr)mp_n^m(\cos\theta_p)e^{-jm\varnothing p} \cdot \frac{4\pi(n+m)!}{(n-m)!} \tag{33}$$

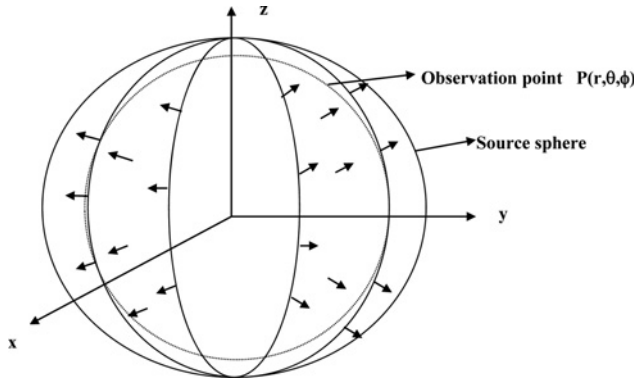

Fig. 5 *Geometry of spherical array of point dipoles*

The suitably normalised functions, denoted by $Y_{lm}(\theta, \varnothing)$ are defined as

$$Y_{lm}(\theta, \varnothing) = \sqrt{\frac{2l+1(l+m)!}{4\pi(l+m)!}}\, P_n^m(\cos\theta)\mathrm{e}^{\mathrm{j}m\varnothing} \tag{36}$$

The spherical harmonics obey the condition [21]

$$Y_{l,-m}(\theta, \varnothing) = (-1)^m Y_{lm}^*(\theta, \varnothing) \tag{37}$$

The normalisation and orthogonality conditions are

$$\int_0^{2\pi} \mathrm{d}\varnothing \int_0^{2\pi} \sin\theta\, \mathrm{d}\theta Y_{l'm'}(\theta, \varnothing) Y_{lm}(\theta, \varnothing) = \delta_{l'l}\delta_{m'm} \tag{38}$$

The complete relation is

$$\sum_{l=0}^{\infty}\sum_{m=-l}^{l} Y_{l'm'}\left(\theta', \varnothing'\right) Y_{lm}^*(\theta, \varnothing) = \delta\left(\varnothing - \varnothing'\right)\delta\left(\cos\theta - \cos\theta'\right) \tag{39}$$

Using the spherical harmonics in (36) on (34), and utilising the orthogonality relation in (38), we can reconstruct the currents of the array.

5 Numerical results and discussions

This section outlines the validation of the reconstruction algorithms that were derived in Sections 2–4. The programmes were written in MATLAB©, and each algorithm was tested in the following two steps:

- Generation of the near-field of the array, at a specified planar, cylindrical or spherical surface, using the direct current-field equation
- Application of the synthesis method (for the planar, cylindrical or spherical array) to reconstruct the electric currents of the array elements.

In the simulation study of all the three cases: planar, cylindrical and spherical arrays, we assumed the current distribution in the array to be uniform, and uniform spacing between array elements.

5.1 Simulation results for a planar array

In this simulation, we have considered a uniformly spaced planar array of 25 (5×5) point electric dipoles with a

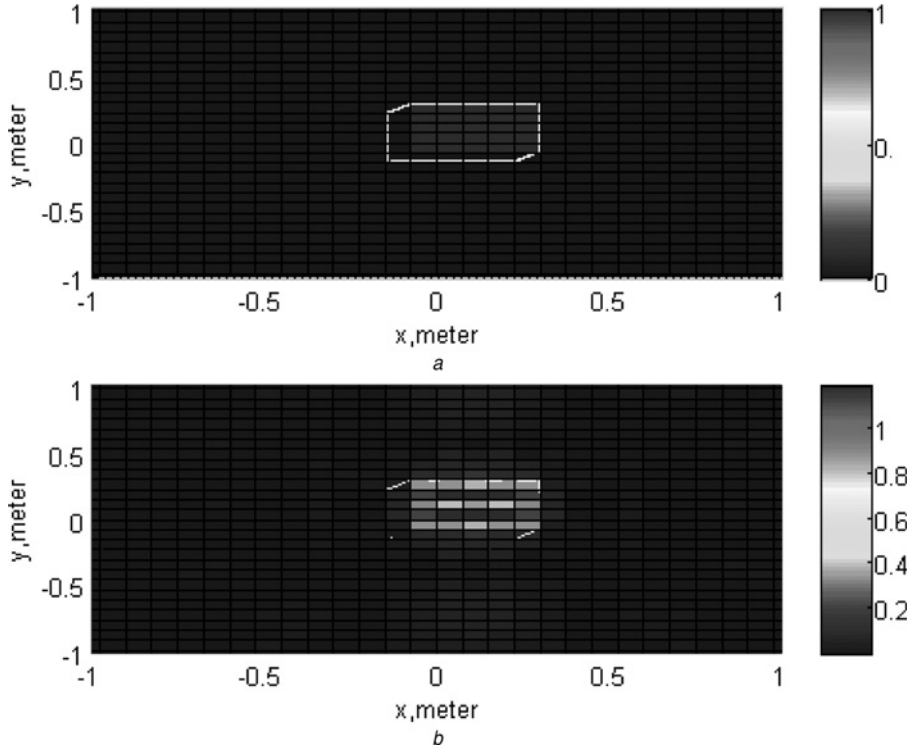

Fig. 6 *Exact and reconstructed currents of planar array*

a Exact
b Reconstructed

doi: 10.1049/iet-map.2012.0208

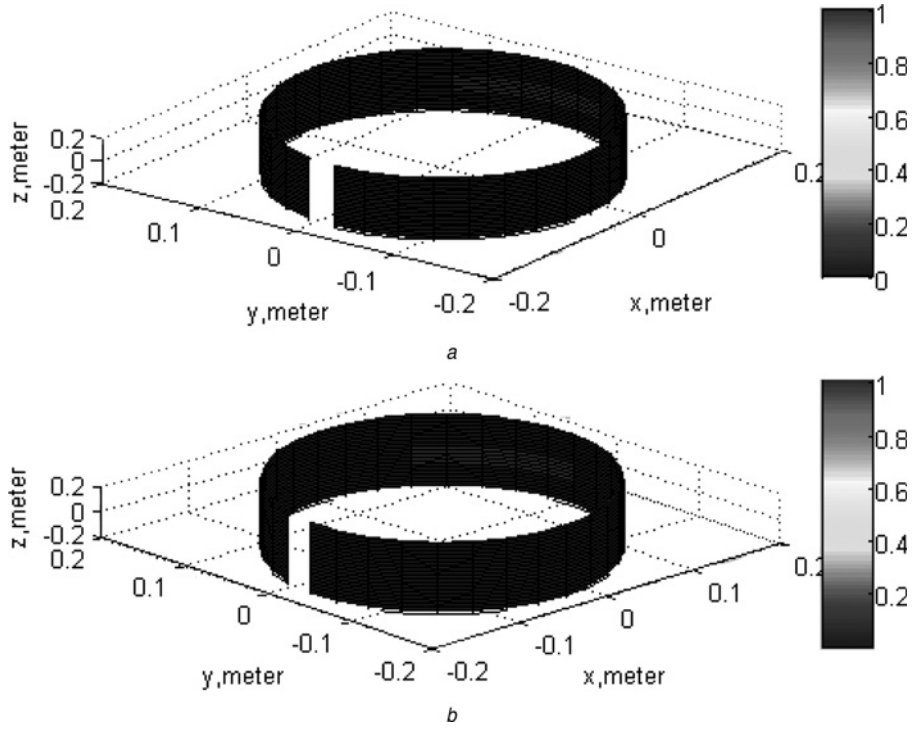

Fig. 7 *Exact and reconstructed currents of cylindrical array*

a Exact
b Reconstructed

current flow direction along the *x*-axis as shown in Fig. 3. The dipoles were assumed to be excited with currents uniform in amplitude and phase, and at a frequency of 1 GHz. In this example, the inter-element spacing along both array axes is $d = 0.25\lambda$. The NF data were generated over a 128×128 point grid, over a parallel observation plane at $z_0 = 0.75\lambda$. The reconstruction algorithm, as detailed in (5)–(8), was implemented to obtain the array currents. The exact array excitation currents employed for generating the NF data and the synthesised array excitation currents are compared in Figs. 6*a* and *b*, respectively, and as observed, a close agreement is noticed between the two values.

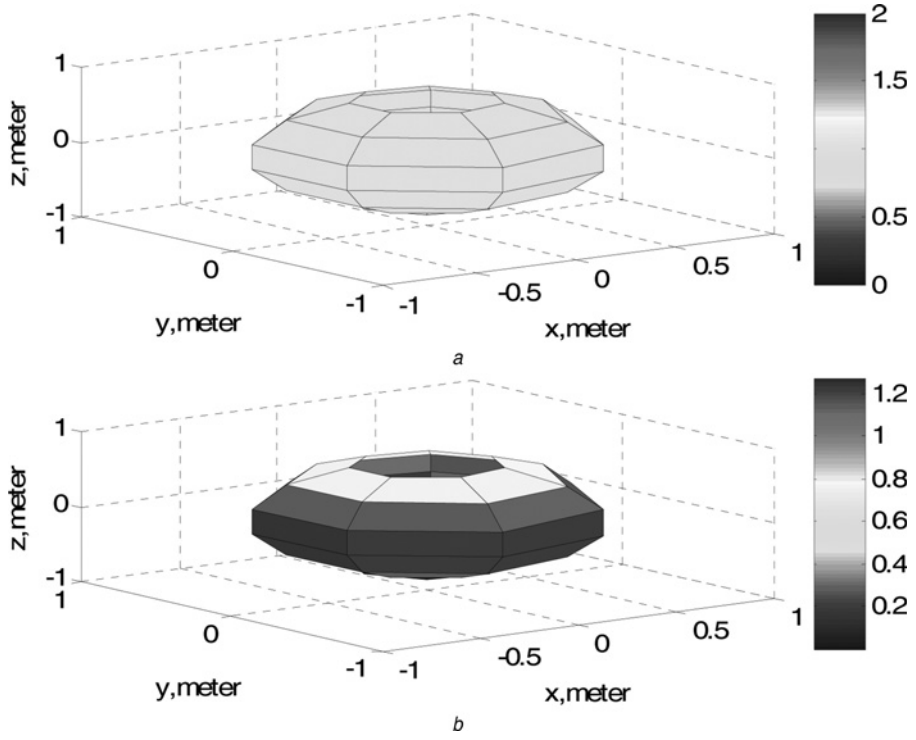

Fig. 8 *Exact and reconstructed currents of spherical array*

a Exact
b Reconstructed

5.2 Simulation results for cylindrical array

In this simulation example, a two-dimensional cylindrical patch array of 25 (5×5) uniformly spaced, point dipoles, with current flowing along the $\hat{z}$-direction. The array structure, as shown in Fig. 4*b*, is assumed with the following dimensions:

Length of array $L = 6\lambda$
Radius of cylindrical array surface $a = 0.5\lambda$
Radius of observation cylindrical surface $= \rho = 0.35\lambda$
Angular spacing $\Delta\phi = ((2\pi)/(32))$ rad $=> 11.25°$
Linear spacing $\Delta z = \lambda/32$
Frequency of array = 1 GHz.

The near-field of the array $E_z(\rho, \varphi, z)$ was utilised to reconstruct the array currents by using the reconstruction algorithm given in (25)–(28). The near-field synthesis performed on the array gave the reconstructed array current distribution, which is depicted in Fig. 7*b*, and compared with the exact array currents in Fig. 7*a*. The colour bar comparison on the right shows that the array currents have been reconstructed with good accuracy, thereby validating the rigorousness of the algorithm.

5.3 Simulation results of spherical array

Finally, the synthesis example was completed for a 49-element (7×7) spherical array of $\hat{\boldsymbol{r}}$-directed point dipoles situated around the surface of the array as shown in Fig. 5. The details of the array are given below:

Radius of array spherical surface $= r_0 = 2.5\lambda$
Radius of application spherical surface $= r = 2\lambda$
Frequency of array = 1 GHz
Array spacing along $\boldsymbol{\phi}$-direction: $\Delta\boldsymbol{\Phi} = ((2\pi)/(7))$ radians
Array spacing along $\boldsymbol{\theta}$-direction: $\Delta\boldsymbol{\theta} = (\pi/7)$ radians.

The array near field was generated over the observation spherical surface, and the synthesis procedure was implemented using (31)–(38). The exact and reconstructed currents are shown in Figs. 8*a* and *b*, respectively, and show good agreement.

6 Conclusions

The main focus of this paper is to design and test efficient reconstruction algorithms for the near-field synthesis of array currents over planar, cylindrical and spherical surfaces. This is a prime requirement in the design of array systems for near-field applications such as RF/microwave hyperthermia in the treatment of tumours. Accurate array current reconstruction is very important to ensure focus of the array beam on the tumour volume, with minimum radiation to adjacent healthy tissue; and conformal array synthesis is essential to deliver radiation to surfaces of the human or animal body with different geometrical profiles. The demonstration of the synthesis procedure was similar for all array geometries: the near field of the array was generated by feeding proper current values to the antennas. Then the currents are reconstructed from field to verify that the reconstructed currents match the currents that were initially fed to the antennas.

All the three array geometries have been simulated and synthesised using MATLAB, and the graphical representation of the simulated code for each array shows the extent to which reconstructed currents match the initial currents. To a large extent, the reconstructed currents and the initial currents have matched for each of the three arrays. The future direction of this work is to test the set of reconstruction algorithms on a practical conformal array system, and gauge the focusing properties and capability of the array to control the focus point over a desired region.

7 References

1 American Cancer Society: 'Progress Report on Reducing the Global Cancer Burden'. Presented at the 20th World Cancer Congress, August 2008
2 Bansal, R.: 'Battling cancer: the latest on microwave hyperthermia', *IEEE Microw. Mag.*, 2005, **6**, (3), pp. 32–34
3 Jones, E.L., Oleson, J.R., Prosnitz, L.R., *et al.*: 'Randomized trial of hyperthermia and radiation for superficial tumors', *J Clin. Oncol.*, 2005, **23**, (13), pp. 3079–3085
4 Kumar, B.P., Karnik, N., Branner, G.R.: 'Near-field beam-forming for hyperthermia applications using waveguide aperture arrays (Invited Paper)'. Proc. of the 2002 Progress in Electromagnetics Research (PIERS) Conf., Boston, July 2002, pp. 345 (Abstract)
5 Tulpule, R., Karnik, N., Kumar, B.P., Branner, G.R.: 'Near-field beamforming in conformal linear arrays'. Proc. 2002 IEEE Antennas and Propagation Society Int. Symp., San Antonio, Texas, July 2002, pp. 120–123
6 Karnik, N., Shah, P., Kumar, B.P., Branner, G.R.: 'Near-field beamforming in conformal planar arrays'. Proc. 2002 IEEE Antennas and Propagation Society Int. Symp., San Antonio, Texas, July 2002, pp. 114–117
7 Narasimham, M.S., Kumar, B.P. : 'A technique of synthesizing the excitation currents of planar arrays or apertures', *IEEE Trans. Antennas Propag.*, 1990, **38**, (9), pp. 1326–1332
8 Sanchez, D., Baquero, M., Vico, F., Bernardo, B.: 'Detection of defective elements in an X band array antenna from its near field measurements'. Proc. 2007 Antennas and Propagation Society Int. Symp., pp. 1637–1640
9 Iglesias, R., Ares, F., Fernandez-Delgado, M., Rodriguez, J., Bregains, J., Barro, S.: 'Element failure detection in linear antenna arrays using case-based reasoning', *IEEE Antennas Propag. Mag.*, 2008, **50**, (4), pp. 198–204
10 Leibfritz, M.M., Landstorfer, F.M., Eibert, T.F.: 'An equivalent source method to determine complex excitation levels of antenna arrays from near-field measurements'. The Second European Conf. on Antennas and Propagation, 2007. EuCAP 2007, 2007, pp. 1–7
11 Laurin, J.-J., Zurcher, J.-F., Gardiol, F.E.: 'Near-field diagnostics of small printed antennas using the equivalent magnetic current approach', *IEEE Trans Antennas Propag.*, 2001, **49**, (5), pp. 814–828
12 Correia, D., Kok, H.P., de Greef, M., Bel, A., van Wieringen, N., Crezee, J.: 'Body conformal antennas for superficial hyperthermia: the impact of bending contact flexible microstrip applicators on their electromagnetic behavior', *IEEE Trans. Biomed. Eng.*, 2009, **56**, (12), pp. 2917–2926
13 Stauffer, P.R., Maccarini, P.F.: 'Evolution of antenna performance for applications in thermal medicine'. Proc. Fifth European Conf. on Antennas and Propagation (EUCAP), 2011, pp. 3080–3083
14 Blekinge Antenna Technology Sweden AB, Specifications Manual, 1st August 2011, available at http://batsab.com/proshow.asp?id=156
15 Karnik, N.S., Tulpule, R., Shah, M., *et al.*: 'Design, simulation and experimental study of near-field beamforming techniques using conformal waveguide arrays', *IET, Microw. Antennas Propag.*, 2010, **4**, pp. 162–174
16 Grbic, A., Merlin, R.: 'Near-field focusing plates and their design', *IEEE Trans. Antennas Propag.*, 2008, **56**, (10), pp. 3159–3165
17 Kumar, B.P.: 'Synthesis of near-field patterns of a class of two-dimensional array antennas'. PhD thesis, Indian Institute of Technology, Madras, India, 1992
18 Balanis, C.A.: 'Antenna theory: analysis and design' (John Wiley & Sons, New York, 1997)
19 Kumar, B.P., Branner, G.R.: 'Generalized analytical technique for the synthesis of unequally spaced arrays with linear, planar, cylindrical or spherical geometry', *IEEE Trans. Antennas Propag.*, 2005, **53**, (2), pp. 621–634
20 Kumar, B.P., Branner, G.R.: 'Near-field analysis of conformal loop arrays', *IEEE Trans. Antennas Propag.*, 1996, **44**, pp. 1428–1429
21 Stratton, J.A.: 'Electromagnetic theory', IEEE Press Series on Electromagnetic Wave Theory' (Wiley-IEEE Press, 2007)